




Graphene-based thermally conductive material cross-linked by poly(ethylenimine) with high thermal and mechanical properties

Wenqiang Xu^{1,2}, Abiola Ganiyat Olatoye^{1,2}, and Yanbin Cui^{1,2,*} 

¹ State Key Laboratory of Multiphase Complex Systems, Institute of Process Engineering, Chinese Academy of Sciences, Beijing 100190, China

² University of Chinese Academy of Sciences, Beijing 100049, China

Received: 14 February 2023

Accepted: 24 May 2023

Published online:
5 June 2023

© The Author(s), under exclusive licence to Springer Science+Business Media, LLC, part of Springer Nature 2023

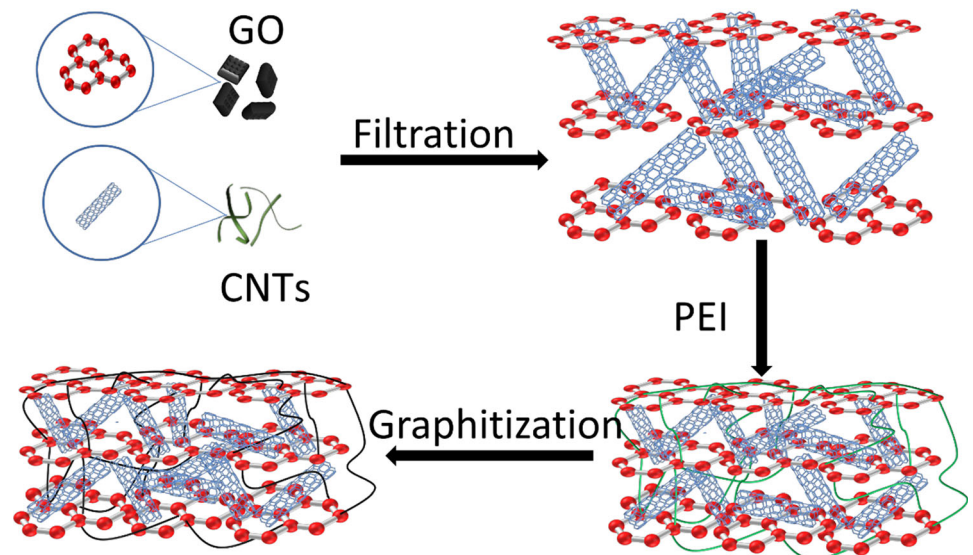
ABSTRACT

In recent decades, graphene has become a very promising thermal management material due to its excellent thermal performance and flexibility. The interaction between adjacent graphene nanosheets, on the other hand, is Van der Waals, limiting the improvement of thermal performance and flexibility of graphene-based heat-conducting films. In this work, a poly(ethylenimine) (PEI)/graphene oxide (GO) /carbon nanotubes (CNTs) heat-conducting film was fabricated, in which PEI acts as a cross-linking agent to form cross-links between GO nanosheets, followed by carbonization and graphitization. Further investigations illustrate that the graphitized PEI/GO/CNTs film has excellent mechanical properties with a tensile strength of 198.3 ± 15.6 MPa and excellent thermal performance with an in-plane thermal conductivity of 1038.4 ± 25.07 W m⁻¹ K⁻¹ and a through-plane thermal conductivity of 7.14 ± 0.25 W m⁻¹ K⁻¹. The graphene-based thermal conducting films have great potential in various fields, such as electronics, aerospace, 5G, etc.

Handling Editor: Jaime Grunlan.

Address correspondence to E-mail: ybcui@ipe.ac.cn

GRAPHICAL ABSTRACT



Introduction

The rapid expansion of electronic equipment, aerospace, 5G, and other technologies has raised the requirements for thermal interfacial materials (TIMs), necessitating not only higher thermal conductivity but also outstanding flexibility [1, 2]. There is a “10 °C Law” for thermal management, which states that every 10 °C increase in temperature reduces the performance of electronic equipment by half [3]. Previous research indicates that the current rate of electronic equipment failure due to heat dissipation difficulties is as high as 55% [3]. Among various TIMs, graphene has great potential in thermal management because of its excellent thermal performance (in-plane thermal conductivity of $5300 \text{ W m}^{-1} \text{ K}^{-1}$) [4, 5] and mechanical property (tensile strength of 125 GPa) [6]. Heat conduction along graphene’s (a honeycomb-like two-dimensional planar structure created by carbon atoms via sp^2 hybridization) surface, for example, can be transported efficiently via lattice vibrations. As a result, graphene is designed to have extremely high in-plane thermal conductivity (κ_{\parallel}) [7]. The C atoms in graphene are connected to three

adjacent C atoms by strong covalent bonds, resulting in graphene with excellent mechanical properties [8]. However, the mechanical properties and thermal conductivity of graphene films are significantly lower than its theoretical values in practical applications [9–11]. This is because graphene thermally conductive films are usually made by a large quantity of graphene nanosheets between which the interfacial interaction is weak, a large amount of phonon scatterings will be induced [12]. Therefore, the in-plane thermal conductivity and mechanical property are significantly reduced. In addition, graphene is typically stacked, with graphene layers connected by van der Waals forces and no phonon transmission channels. Therefore, the through-plane thermal conductivity (κ_{\perp}) of graphene is confined within $0.1\text{--}2 \text{ W m}^{-1} \text{ K}^{-1}$ [7]. Chen et al. fabricated a graphene film through annealing, of which the κ_{\parallel} could achieve $1043.5 \text{ W m}^{-1} \text{ K}^{-1}$, however, the κ_{\perp} was only $0.09 \text{ W m}^{-1} \text{ K}^{-1}$ [13]. To address the anisotropy of graphene, Jia et al. obtained a composite membrane of rGO and CNTs by vacuum filtrating, in which CNTs were inserted into rGO layers to work as heat-transferring channel along through-plane direction and the ultimate κ_{\perp} reached $6.27 \text{ W m}^{-1} \text{ K}^{-1}$ [14].

Although prior studies have made considerable progress in improving the thermal properties of carbon-based TIMs, as electronics evolve, the κ and flexibility of TIMs are necessary for further improvement, which is influenced by the interfacial interaction between adjacent GO nanosheets. There are numerous contact sites between adjacent GO nanosheets during the self-assembly process, which are linked by weak interfacial interactions [12]. In this case, the as-produced thermal conductive films lack flexibility, and further thermal conductivity development of GO-based materials is hampered by the poor connection between GO nanosheets [15–18]. As a result, a correct approach for connecting adjacent GO nanosheets should be used for higher κ and more good flexibility. Salavagione et al. successfully crosslinked GO nanosheets by esterifying the hydroxyl groups of poly(vinyl alcohol) and the carboxyl groups of GO nanosheets, increasing the mechanical property of the resulting GO film by 70% [19]. Even though GO contains many epoxy groups in addition to carboxyl groups, the esterification reaction cannot fully utilize the oxygen-containing groups on GO nanosheets to form adequate interactions. Li et al. successfully grafted octadecylamine molecules onto GO by covalent bond using the reaction between the amino groups at the end of octadecylamine and the oxygen-containing groups on GO. The resulting films' flexibility, conductivity, and thermal conductivity were enhanced [20]. Nonetheless, because octadecylamine is difficult to dissolve in water, the difficulty and cost of preparing thermal conductivity films are surely increased. Polyethyleneimine (PEI), on the other hand, dissolves well in water and contains sufficient primary and secondary amines that can undertake nucleophilic substitution reactions with epoxy groups and amidation reactions with carboxyl groups [21, 22], thereby connecting adjacent GO nanosheets [23, 24]. Furthermore, after heat treatment, PEI can be carbonized, providing stable linkages and a heat transmission channel between adjacent nanoplates [25]. As a result, PEI is an excellent crosslinker for enhancing the interaction of GO nanosheets.

In this work, PEI/GO/CNTs (PGC) films with high thermal conductivity and flexibility are fabricated through a simple vacuum filtration process. GO is selected to act as an in-plane heat-transferring channel due to its ultrahigh in-plane thermal conductivity. CNTs are inserted into GO layers for through-

thickness heat conduction because of their extreme axial thermal performance. PEI works as a cross-linking agent to enhance the interfacial interaction between GO nanosheets. Infrared spectroscopy and X-ray diffraction patterns (XRD) indicated the successful bridging of PEI between GO and CNTs. XRD and Raman's spectroscopy revealed that PGC was flawless and highly crystalline after carbonization at 900 °C (PGC-900) and graphitization at 2800 °C (PGC-2800). The PGC-2800's final in-plane thermal conductivity and through-plane thermal conductivity were 1038.4 ± 25.07 and $7.14 \pm 0.25 \text{ W m}^{-1} \text{ K}^{-1}$, respectively. PGC-2800 also has a tensile strength of $198.3 \pm 15.6 \text{ MPa}$. The newly obtained flexible PGC-2800 film with high thermal conductivity has a promising future in the field of thermal management.

Experimental section

Materials

GO aqueous dispersion (2 wt%) produced by the modified Hummers method is purchased from Ketan New Materials Co., Ltd. (Xiamen, China). CNTs (purity > 98 wt%, diameter 5–15 nm, length 10–30 μm) are provided by Aladdin Biochemical Technology Co., Ltd. (Shanghai, China). PEI (MW600, purity > 99%) is supplied by McLean Biochemical Technology Co., Ltd. (Shanghai, China). Deionized water is produced by the ultra-pure water machine (UPT-I-10 T, ULUPURE, Sichuan, China). All the chemicals have not been further processed.

Fabrication of PGC film

The PGC film was prepared by the self-assembly method during vacuum filtration. The detailed preparation steps are as follows (Fig. 1): Firstly, the GO and CNT powders were mixed into 80 ml of deionized water with a mass ratio of 4:1, and the GO/CNT mixed aqueous dispersion was obtained after ultrasonification (500 W) for 30 min. Secondly, the as-prepared mixed aqueous dispersion was poured onto a filtration paper (Nylon-66, 0.45 μm in pore size) for fabricating a GO/CNT hybrid film (GC) by vacuum self-assembly. Following that, a 0.02 g/ml PEI aqueous solution was decanted into the suction cup to connect the GO and CNTs. The filter cake was transferred to a baking oven for drying at 65 °C for

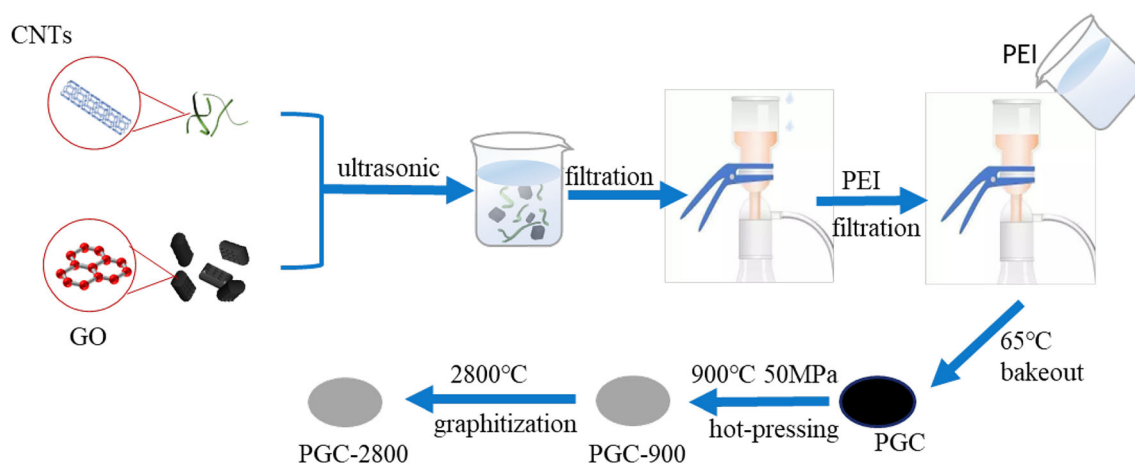


Figure 1 Preparation diagram of PGC-2800 films.

3 h. And finally, a PGC film was obtained after detaching the filter membrane.

Carbonization, graphitization, and reduction were performed to improve the thermal conductivity of PGC films. Firstly, vacuum hot pressing was operated at 900 °C and 50 MPa for 2 h to obtain carbonized and partly reduced PGC films (PGC-900), in which rGO nanosheets were obtained because most oxygen-containing groups were eliminated and PEI was carbonized to nitrogenous carbon [26, 27]. Afterwards, the as-obtained PGC-900 film was graphitized in Ar at 2800 °C for 4 h, during which structural defects were decreased because of the rearrangement of carbon atoms. Finally, the hot-pressing process was repeated to eliminate the voids caused by CO₂ and CO escaping, and the graphitized PGC films (PGC-2800) were obtained. For comparison, the GC film without PEI modification and pure GO film were prepared with the same procedure as the PGC film, followed by graphitization at 2800 °C (GC-2800 and rGO-2800, respectively).

Characterization methods

The scanning electronic microscope (SEM, JSM-6700F, JEOL, Japan) with an acceleration voltage of 5 kV was used to investigate the morphologies and cross-sectional images of various heat-conducting films. The thickness of GO nanosheets was recorded using an atomic force microscope (AFM, MultiMode 8, Bruker, Germany). X-ray diffraction (XRD, Rigaku SmartLab 9Kw, RIGAKU, Japan) was used in conjunction with Cu K radiation ($\lambda = 0.154$ nm) to characterize the crystallinity of heat-conducting films at

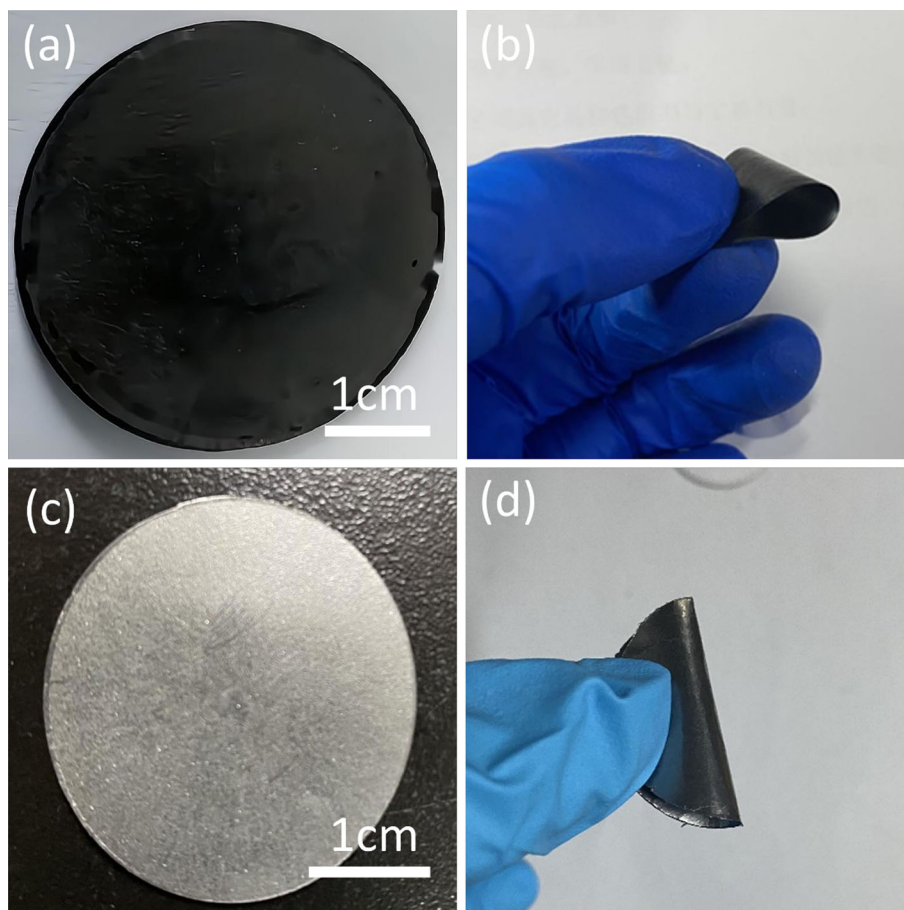
various stages of processing. The defects of the films before and after annealing were compared via Raman spectroscopy (Raman, inVia, Renishaw, UK) with a laser wavelength of 523 nm. FTIR spectrum (Tensor 27, Bruker, Germany) was utilized to study the variation of the chemical bonds of PGC, PGC-900, and PGC-2800 films. The chemical composition of PGC and PGC-900 films was recorded using X-ray photoelectron spectroscopy (XPS, K-Alpha, Thermo Scientific, US) with bandspot, operating voltage and filament current of 400 μ m, 12 kV and 6 mA, respectively. The spectrum decomposition was performed using the Avantage program with Gaussian functions after subtraction of a Shirley background. The tensile strengths of PGC-2800 and GC-2800 films were tested by a dynamic thermomechanical analyzer (DMA, Q800, TA instruments, US). The thermal conductivity of different heat-conducting films was measured using a thermal conductivity analyzer (TPS2500S, Hot Disk, Germany).

Results and discussion

Morphology characterization

The macroscopic images of various PGC, PGC-900 and PGC-2800 are presented in Fig. 2. The films are flattened rounds and appear black before heat treatment, whereas they are silvery gray with a metallic luster after annealing. Figure 2b and d show that the films modified by PEI exhibit excellent flexibility before and after heat treatment. Fig. S1 is the AFM image of GO with a thickness of 1.01 nm, which

Figure 2 Exterior image (a) and flexibility demonstration (b) of PGC film. Digital images of PGC-900 films (c). Flexibility demonstration of PGC-2800 film (d).

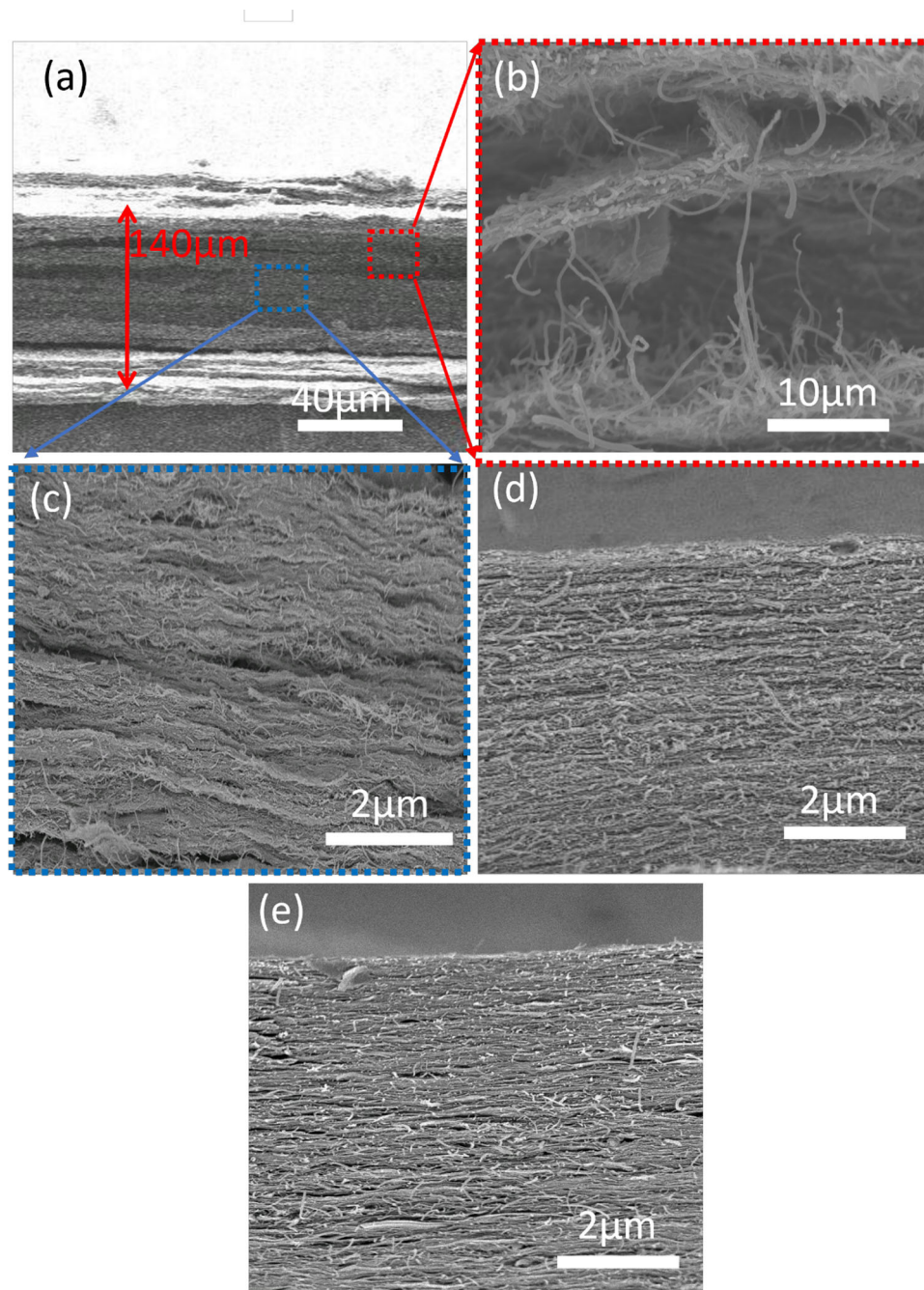


suggests that the GO nanosheets can be considered as a single layer after adequate sonication [28]. The SEM images of the cross-section of the PGC, PGC-900 and PGC-2800 films are shown in Fig. 3. The PGC film has a thickness of 140 μm and possesses an obvious highly aligned layered lamellar structure (Fig. 3a). Also, high-magnification SEM image of PGC film (Fig. 3b) suggests that CNTs are inserted in GO layers, and part of the CNTs can connect the adjacent GO layers, which can act as through-plane thermal transfer channels to improve the through-plane thermal conductivity. It is worth noting that some large gaps (the red and blue squares in Fig. 3a) appear in the layer structure of the PGC film. Furthermore, there are numerous small holes in the PGC film (Fig. 3c). These large gaps and small holes are due to water evaporation during the drying process and are harmful to the thermal performance of heat-conducting films. Figure 3d, e show that the pores of PGC-900 and PGC-2800 become smaller after hot pressing and graphitization, especially the lamellae in PGC-2800 are more tightly connected.

Structural characterization

The chemical groups of PGC films and the interactions of PEI with GO were evaluated by FTIR spectroscopy (Fig. 4). As shown in Fig. 4, the absorption peaks at 3434, 1719, and 1622 cm^{-1} are assigned to the stretching vibrations of -OH, C = O, and C = C, respectively. Also, the characteristic peak of the epoxy group (C-O-C) appears at 1051 cm^{-1} . In comparison to the GO films, the PGC film's FTIR spectroscopy shows that the peak at 1719 cm^{-1} of C = O disappeared as the amino groups at the end of PEI perform amidation reactions with the carboxyl groups of GO nanosheets, while the peak intensity of C-O-C at 1051 cm^{-1} was reduced. Interestingly, two new peaks for PGC films assigned to C-N and N-H appear at 1451¹ and 1568 cm^{-1} respectively, due to the reaction between the amino groups of PEI and the epoxy groups of GO nanosheets [29]. The peaks of C-N and N-H reveal that PEI has been successfully grafted to GO nanosheets.

Figure 3 SEM images of the cross sections of PGC films at low (a) and high magnification (b, c), PGC-900 films (d), PGC-2800 (e).



XPS was employed to further confirm the successful grafting of PEI to GO and reveal the evolution of oxygen-containing groups in PGC and PGC-900 films. The XPS spectrum (Fig. 5a) shows that there are only carbon (C1s) and oxygen (O1s) peaks in GC films. The peak of nitrogen (N1s) appears in PGC films, and the ratio of carbon to oxygen (C/O) of PGC films (5.38) is increased compared with GC films (2.24), demonstrating that PEI successfully is inserted to GO. It is worth noting that the C atom ratio

dramatically increases from 76.80% for PGC film to 91.26% for PGC-900 film, the O atom ratio notably decreases to 5.12% for PGC-900 film from 14.27% for PGC film, and the N atom ratio has a reduction from 8.93% for PGC film to 3.62% for PGC-900 (Table 1). This is due to the removal of oxygen functional groups from GO as well as the escape of the N element from PEI in the form of NH_3 , HCN, and other compounds during the carbonization process at 900 °C, respectively [26]. When annealing at a higher

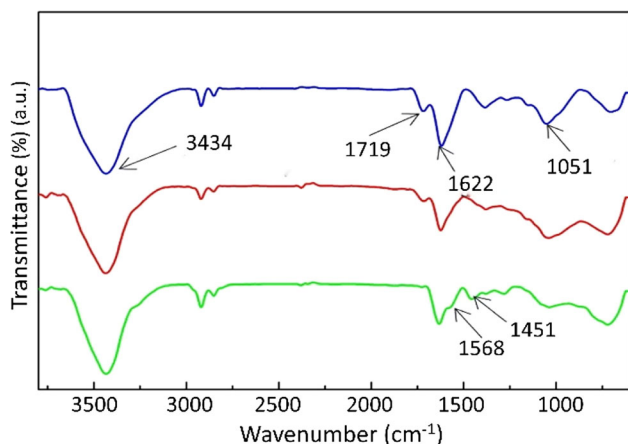


Figure 4 FTIR spectra of GO, GC, and PGC films.

Table 1 Parameter summary of XPS spectrum of films

Sample	GC	PGC	PGC-900	PGC-1600	PGC-2800
C%	69.15	76.80	91.26	95.19	96.51
O%	30.85	14.27	5.12	1.46	0.63
N%	–	8.93	3.62	3.35	2.86
C/O	2.24	5.38	17.82	65.20	153.19

temperature, the O and N content both have a further reduction.

To investigate the connection between PEI and GO, the C1s spectrum of GC was fitted into four peaks with different bonding energies [14]: C–C (284.8 eV),

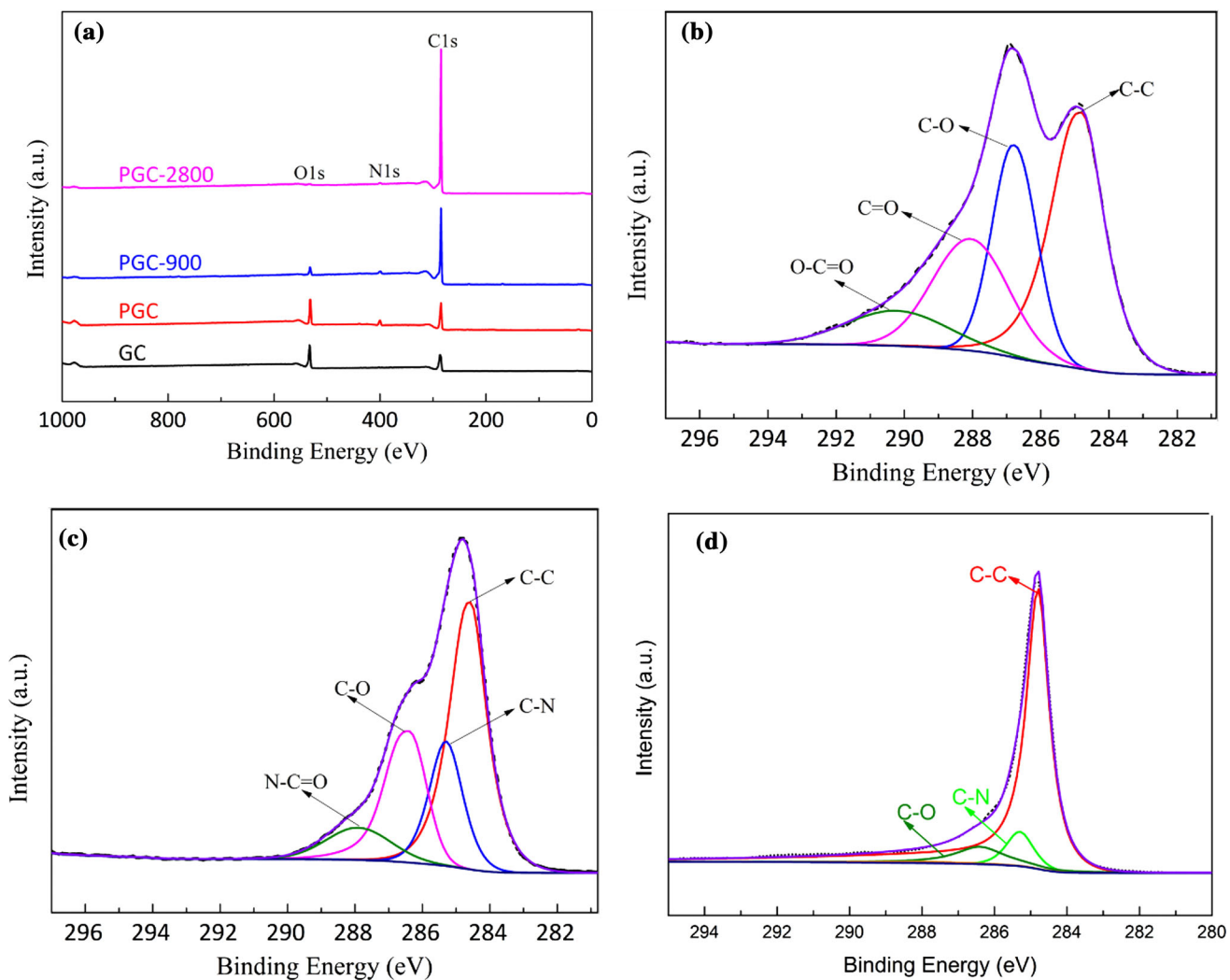


Figure 5 a XPS spectrum of the GC, PGC, PGC-900, PGC-1600 and PGC-2800 films. C1s XPS spectrum in b GC films, c PGC films and d PGC-2800 films.

C–O (286.4 eV), C = O (288.1 eV), and O = C–O (289.2 eV) (Fig. 5b), and four different peaks were fitted from the C1s spectrum of the PGC film: C–C (284.8 eV), C–N (285.3 eV), C–O (286.4 eV), and O = C–N (287.9 eV) (Fig. 5c). Also, the C–O peak intensity of PGC films (Fig. 5c) decreases when compared to GC films (Fig. 5b), and two new peaks (C–N and O = C–N) appear after PEI grafting. This is due to the reaction of carboxyl and epoxy groups in GO with the amine groups in PEI, which is consistent with the results of FTIR spectroscopy. As shown in Fig. 5d, there are C–C (284.5 eV), C–O (286.4 eV) and C–N (285.3 eV) in the C1s spectrum of PGC-2800, the peak intensity of C–O (286.4 eV) and C–N (285.3 eV) is weak, illustrating that the low content of impurity elements in PGC-2800 after graphitization, which is beneficial to the thermal conductivity of PGC-2800.

XRD was utilized to reveal the changes in the crystal structure of GO, GC, and PGC films (Fig. 6). A typical peak at $2\theta = 9.48^\circ$ corresponds to the (001) plane of GO. The interlayer d-spacing (d_{001}) was calculated using Bragg's Law (Equation S1) [30]. The d_{001} of GO is 0.93 nm (Table 2). Furthermore, the peaks of the (001) plane for GC and PGC film move to 7.08° and 7.74° , respectively, whereas the corresponding d_{001} increases to 1.24 and 1.14 nm. This illustrates that the insertion of CNTs increases the d_{001} of GO, but the cross-linking of PEI reduces the d_{001} of GO to a certain extent, revealing the bridging role of PEI between adjacent GO layers [31]. Compared with GC films, the peak for the (001) plane of PGC films broadens, indicating that the addition of

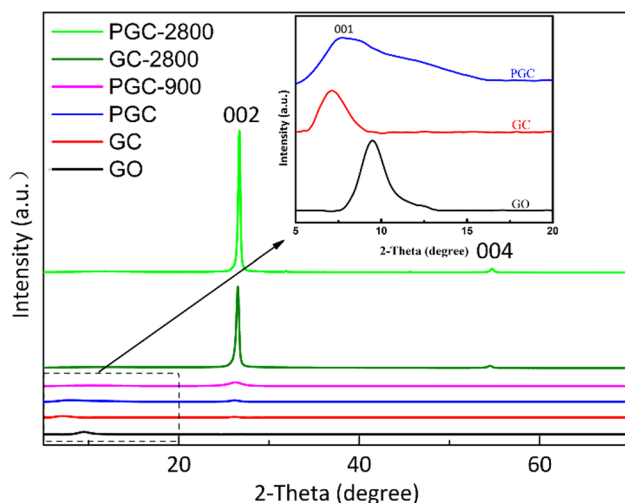


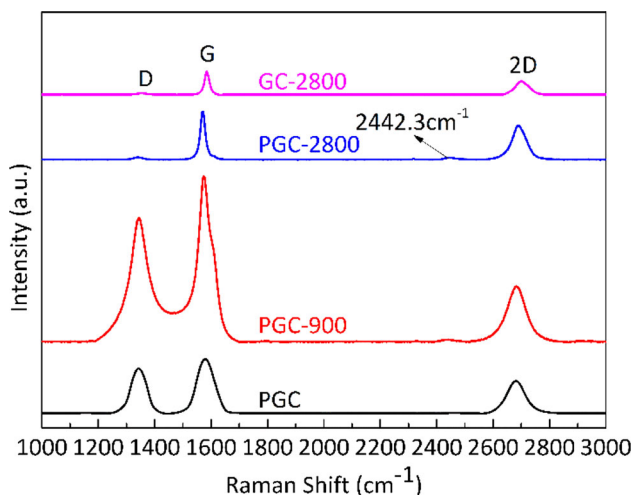
Figure 6 XRD patterns of GO, GC, PGC, PGC-900 and PGC-2800 films.

PEI reduces crystallinity. In Fig. 6b, the peak intensity for the (002) plane of graphite ($2\theta = 26.5^\circ$) rises with the increasing annealing temperature. The interlayer d-spacing of the (002) plane (d_{002}) decreases from 0.338 nm of PGC films to 0.333 nm of PGC-2800 films (Table 2). It is worth noting that the d_{002} of PGC-2800 films is less than that of natural graphite (0.335 nm), which further demonstrates that the eaddition of PEI can help to shorten the distance of adjacent GO layers for higher through-plane thermal conductivity. The crystallite dimension along the vertical crystal plane direction (L_c) of PGC-2800 and GC-2800 were calculated through the Scherrer Equation (Equation S2) [32]. The result displays that the L_c of PGC-2800 is 25.24 ± 3.3 nm, higher than that of GC-2800 (18.56 ± 2.1 nm), illustrating the connection of PEI between rGO layers.

Raman spectroscopy was utilized to investigate the crystal structure defects of PGC films. As displayed in Fig. 7, the peaks at 1350 , 1581 , and 2698 cm^{-1} correspond to the D band, G band, and 2D band, respectively. The D band is connected with disordered carbon structure, including defects and oxygen-containing functional groups, while the G band is associated with the degree of graphitization (sp^2 hybridization), and the 2D band is related to the existence of crystalline carbon in CNTs (Fig. S4) [32, 33]. As the annealing temperature rises, the D peak weakens dramatically; at 2800°C , the D peak almost disappears, and the ratio of I_D/I_G decreases sharply (Table 3). The value of I_D/I_G for PGC-2800 is reduced to 0.05, and the I_D/I_G for PGC is 0.826, demonstrating that defects in PGC have been removed basically with annealing. Notably, there is a new peak at 2442.3 cm^{-1} corresponding to nitrogenous carbon originating from the carbonization of PEI in the hot-pressing stage at 900°C [26]. This indicates that PEI exists in PGC film in the form of nitrogenous carbon after carbonization, which is consistent with the results of XPS. To study the changes in crystallite size (L_a) with the annealing temperature, the values of L_a (Table 4) are calculated by Cançado Equation [34] (Equation S3). L_a increases as the annealing temperature rises. For example, L_a of PGC-2800 is raised to 384.40 ± 15.84 nm, while it is 23.27 ± 2.01 nm for PGC film, illustrating that there is a highly crystallization along the in-plane direction after eannealing at 2800°C [14]. Compared with GC-2800, the value of L_a in PGC-2800 rises from 305.10 ± 10.56 to 384.40 ± 15.84 nm, suggesting that

Table 2 The parameter of XRD of GO, GC, PGC, PGC-900, and PGC-2800 films

Sample	2 θ (001)	2 θ (002)	d ₀₀₁ (nm)	d ₀₀₂ (nm)	Lc (nm)
GO	9.48°	–	0.93	–	–
GC	7.08°	–	1.24	–	–
PGC	7.74°	26.29°	1.14	0.338	–
PGC-900	–	26.46°	–	0.336	–
PGC-2800	–	26.7°	–	0.333	25.24 \pm 3.3
GC-2800	–	26.50°	–	0.336	18.56 \pm 2.1

**Figure 7** Raman spectrum of PGC, PGC-900, PGC-1600, and PGC-2800 films.

the addition of PEI can promote the assembly of graphene after carbonization.

To further prove the connection of PEI to GO nanosheets, PGC and GC films were immersed in deionized water for a few days. As shown in Fig. S2, the GC film had an apparent expansion in thickness and started to disintegrate on the second day after being placed in water. On the fifth day, the water bath became turbid with a slight shaking. However, the water bath of the PGC film was clear until the fifth day. In the absence of effective cross-linking between adjacent graphene sheets, GC films are highly unstable, and PEI can indeed connect the neighboring graphene nanoplates [31].

Table 3 The digital information of Raman spectroscopy

Sample	PGC	PGC-900	GC-2800	PGC-2800
I _D : I _G	0.83	0.76	0.063	0.050
La(nm)	23.27 \pm 2.01	27.86 \pm 3.78	305.10 \pm 10.56	384.40 \pm 15.84

Flexibility and thermal conductivity

DMA was utilized to investigate the mechanical properties of PGC, PGC-900, PGC-2800, GC-2800 and rGO-2800 films (Fig. 8). As the ramp force increased at a rate of 0.5 N/min, the films were gradually stretched. The tensile strength of PGC film is 26.8 \pm 3.2 MPa (Table 4). After graphitization, the tensile strength of PGC-2800 film rises sharply to 198.3 \pm 15.6 MPa. This is because the rearrangement of C atoms during graphitization and more C atoms to be covalently attached. With the influence of CNTs, the tensile strength of GC-2800 film is 83.9 \pm 7.5 MPa, higher than that of rGO-2800 (32.56 \pm 3.5 MPa). It is worth noting that the tensile strength of PGC-2800 film is about 2.4 times higher than that of GC-2800. Flexibility refers to the amount of energy absorbed before destroyed. In DMA test, the area of integration of the stress–strain curve corresponds to the amount of energy absorbed by the material before damage [35]. As shown in Fig. 8, PGC-2800 is apparently more flexible than GC-2800. During the graphitization process, C atoms in PEI are activated to participate in C-atom rearrangement, promoting covalent linkage between adjacent rGO nanosheets, resulting in a substantially stronger connection between rGO nanosheets and leading to excellent mechanical properties of PGC-2800 [14].

Using a thermal constant analyzer, the thermal performance of as-obtained PGC films with varied annealing temperatures was examined (Fig. 9). Figure 9a and b show that the in-plane thermal conductivity of PGC film increases drastically with increasing annealing temperature, from 3.26 \pm 0.15 W m⁻¹ K⁻¹ for PGC to

$1038.4 \pm 25.07 \text{ W m}^{-1} \text{ K}^{-1}$ for PGC-2800, and the through-plane thermal conductivity increases to $7.14 \pm 0.25 \text{ W m}^{-1} \text{ K}^{-1}$ for PGC-2800 from $0.055 \pm 0.0032 \text{ W m}^{-1} \text{ K}^{-1}$ for PGC films, respectively. It is due to the annealing process's elimination

Table 4 The digital information of DMA

Sample	Stress (MPa)	Strain (%)
GC-2800	83.9 ± 7.5	0.835
rGO-2800	32.56 ± 3.5	0.344
PGC-2800	198.3 ± 15.6	1.458
PGC-900	54.7 ± 4.6	0.536
PGC	26.8 ± 3.2	0.494

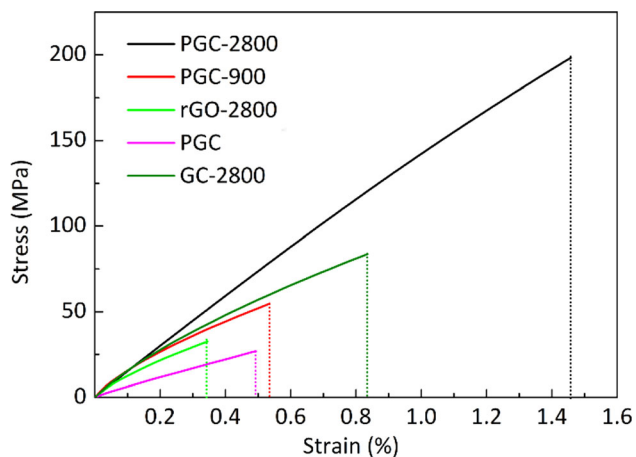


Figure 8 Mechanical properties of GC-2800 and PGC-2800 films.

of oxygen-containing functional groups and restoration of crystal structure [36]. Compared with the GC-2800 films, PGC-2800 films exhibits higher κ_{\perp} , as a result of the connection between adjacent rGO nanosheets via carbonized PEI [12], and both PGC-2800 and GC-2800 exhibit lower κ_{\parallel} than that of pure rGO films (rGO-2800). In the in-plane direction, the addition of CNTs affects the GO alignment to some extent and thus reduces the κ_{\parallel} of GO films [37].

In addition, the mechanical and thermal performance of PGC films were compared with various studies (Table S1). The reported carbon-based thermal conducting films have excellent in-plane thermal conductivity. However, either the κ_{\perp} or mechanical performance of the reported carbon-based thermal conducting films has been always been limited, which impedes their practical application in flexible electronic equipment with increasing power density. Herein, PEI was used as a bridge to cross-link adjacent GO nanosheets for improving κ_{\perp} and the mechanical performance of PGC films based on guaranteeing high in-plane thermal conductivity.

Conclusion

In conclusion, a simple self-assembly method was used to fabricate a graphene-based thermal conducting film (PEI/GO/CNTs) with superior thermal performance ($\kappa_{\parallel} = 1038.4 \pm 25.07 \text{ W m}^{-1} \text{ K}^{-1}$, $\kappa_{\perp} = 7.14 \pm 0.25 \text{ W m}^{-1} \text{ K}^{-1}$) and mechanical properties (the tensile strength of $198.3 \pm 15.6 \text{ MPa}$). rGO guarantees ultrahigh in-plane thermal conductivity, and the insertion of CNTs provides channels for

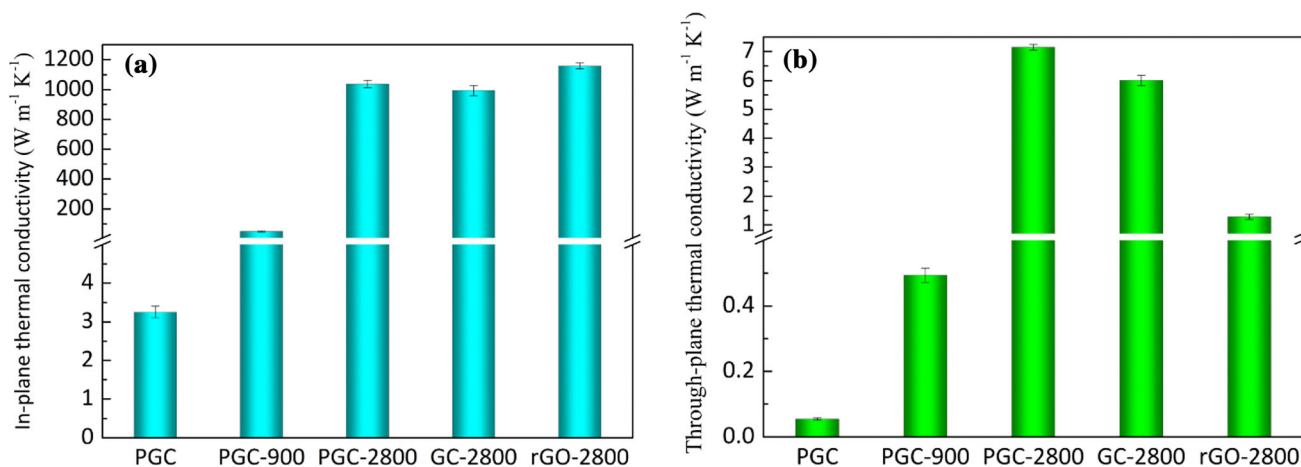


Figure 9 Thermal conductivities of PGC, PGC-900, PGC-1600, PGC-2800, GC-2800, and rGO-2800 films.

through-plane heat conduction. Carbonized PEI enhances the interfacial interaction between rGO nanosheets, thus reducing the interfacial thermal resistance and enhancing the mechanical performance of graphitized PGC films. Compared with GC-2800 films, the κ_{\parallel} and κ_{\perp} of PGC-2800 films are increased by 4.4 and 18.8%, respectively.

Data and code availability

The data that support the findings of this study are available on request from the corresponding author.

Author contribution

WX: Investigation, Formal analysis, Data curation, Writing—original draft, Validation, Methodology. AGO: Writing—review and editing, Formal analysis, Investigation. YC: Writing—review and editing, Conceptualization, Resources, Project administration, Supervision, Funding acquisition.

Declarations

Conflict of interest The authors declare that there are no competing financial interests.

Supplementary Information: The online version contains supplementary material available at <http://doi.org/10.1007/s10853-023-08635-9>.

References

- [1] Dong Z-j, Sun B, Zhu H, Yuan G-m, Li B-l, Guo J-g, Li X-k, Cong Y, Zhang J (2021) A review of aligned carbon nanotube arrays and carbon/carbon composites: fabrication, thermal conduction properties and applications in thermal management. *New Carbon Mater* 36:873–892. [https://doi.org/10.1016/s1872-5805\(21\)60090-2](https://doi.org/10.1016/s1872-5805(21)60090-2)
- [2] Gao J, Yan Q, Lv L, Tan X, Ying J, Yang K, Yu J, Du S, Wei Q, Xiang R, Yao Y, Zeng X, Sun R, Wong C-P, Jiang N, Lin C-T, Dai W (2021) Lightweight thermal interface materials based on hierarchically structured graphene paper with superior through-plane thermal conductivity. *Chem Eng J* 419:129609. <https://doi.org/10.1016/j.cej.2021.129609>
- [3] Belhardj S, Mimouni S, Saidane A, Benzohra M (2003) Using microchannels to cool microprocessors: a transmission-line-matrix study. *Microelectron J* 34:247–253. [https://doi.org/10.1016/s0026-2692\(03\)00004-1](https://doi.org/10.1016/s0026-2692(03)00004-1)
- [4] Feng C-P, Chen L-B, Tian G-L, Bai L, Bao R-Y, Liu Z-Y, Ke K, Yang M-B, Yang W (2020) Robust polymer-based paper-like thermal interface materials with a through-plane thermal conductivity over 9 Wm⁻¹K⁻¹. *Chem Eng J* 392:123784. <https://doi.org/10.1016/j.cej.2019.123784>
- [5] Balandin AA, Ghosh S, Bao W, Calizo I, Teweldebrhan D, Miao F, Lau CN (2008) Superior thermal conductivity of single-layer graphene. *Nano Lett* 8:902–907. <https://doi.org/10.1021/nl0731872>
- [6] Lee C, Wei X, Kysar JW, Hone J (2008) Measurement of the elastic properties and intrinsic strength of monolayer graphene. *Science* 321:385–388. <https://doi.org/10.1126/science.1157996>
- [7] Zhang J, Shi G, Jiang C, Ju S, Jiang D (2015) 3D bridged carbon nanoring/graphene hybrid paper as a high-performance lateral heat spreader. *Small* 11:6197–6204. <https://doi.org/10.1002/sml.201501878>
- [8] Stankovich S, Dikin DA, Dommett GHB, Kohlhaas KM, Zimney EJ, Stach EA, Piner RD, Nguyen ST, Ruoff RS (2006) Graphene-based composite materials. *Nature* 442:282–286. <https://doi.org/10.1038/nature04969>
- [9] Shen B, Zhai W, Zheng W (2014) Ultrathin flexible graphene film: an excellent thermal conducting material with efficient EMI shielding. *24:4542–4548*. <https://doi.org/10.1002/adfm.201400079>
- [10] Peng L, Xu Z, Liu Z, Guo Y, Li P, Gao C (2017) Ultrahigh thermal conductive yet superflexible graphene films. *29:1700589*. <https://doi.org/10.1002/adma.201700589>
- [11] Kumar P, Shahzad F, Yu S, Hong SM, Kim Y-H, Koo CM (2015) Large-area reduced graphene oxide thin film with excellent thermal conductivity and electromagnetic interference shielding effectiveness. *Carbon* 94:494–500. <https://doi.org/10.1016/j.carbon.2015.07.032>
- [12] Zhu Y, Peng Q, Qin Y, Zhao X, Xu L, Chen Q, Li Y, Xu Z, He X (2020) Graphene-carbon composite films as thermal management materials. *ACS Appl Nano Mater* 3:9076–9087. <https://doi.org/10.1021/acsnm.0c01754>
- [13] Song N, Jiao D, Cui S, Hou X, Ding P, Shi L (2017) Highly Anisotropic thermal conductivity of layer-by-layer assembled nanofibrillated cellulose/graphene nanosheets hybrid films for thermal management. *ACS Appl Mater Interfaces* 9:2924–2932. <https://doi.org/10.1021/acsmi.6b11979>
- [14] Jia H, Kong Q-Q, Yang X, Xie L-J, Sun G-H, Liang L-L, Chen J-P, Liu D, Guo Q-G, Chen C-M (2021) Dual-functional graphene/carbon nanotubes thick film: Bidirectional thermal dissipation and electromagnetic shielding. *Carbon* 171:329–340. <https://doi.org/10.1016/j.carbon.2020.09.017>

- [15] Cui Y, Zhang M (2013) Cross-links in carbon nanotube assembly introduced by using polyacrylonitrile as precursor. *ACS Appl Mater Interfaces* 5:8173–8178. <https://doi.org/10.1021/am4022686>
- [16] Cui Y, Zhang M (2013) Fabrication of cross-linked carbon nanotube foam using polymethylmethacrylate microspheres as templates. *J Mater Chem A* 1:13984. <https://doi.org/10.1039/c3ta13065g>
- [17] Jin Y, Lee W (2019) Cross-linking stabilizes electrical resistance of reduced graphene oxide in humid environments. *Langmuir* 35:5427–5434. <https://doi.org/10.1021/acs.langmuir.8b03416>
- [18] Wang B, Liu J, Yue S, Wang X, Zhang Y, Fu Y, Li T, Wang T (2021) Preparation of graphene/Al composites with a lamellar structure by silane cross-linking graphene oxide. *J Market Res* 13:2433–2441. <https://doi.org/10.1016/j.jmrt.2021.06.009>
- [19] Salavagione HJ, Gómez MA, Martínez G (2009) Polymeric modification of graphene through esterification of graphite oxide and poly(vinyl alcohol). *Macromolecules* 42:6331–6334. <https://doi.org/10.1021/ma900845w>
- [20] Li W, Tang X-Z, Zhang H-B, Jiang Z-G, Yu Z-Z, Du X-S, Mai Y-W (2011) Simultaneous surface functionalization and reduction of graphene oxide with octadecylamine for electrically conductive polystyrene composites. *Carbon* 49:4724–4730. <https://doi.org/10.1016/j.carbon.2011.06.077>
- [21] Jiang F, Zhao W, Wu Y, Wu Y, Liu G, Dong J, Zhou K (2019) A polyethyleneimine-grafted graphene oxide hybrid nanomaterial: synthesis and anti-corrosion applications. *Appl Surf Sci* 479:963–973. <https://doi.org/10.1016/j.apsusc.2019.02.193>
- [22] Tian Y, Xie Y, Dai F, Huang H, Zhong L, Zhang X (2020) Ammonium-grafted graphene oxide for enhanced corrosion resistance of waterborne epoxy coatings. *Surface Coat Technol* 383:125227. <https://doi.org/10.1016/j.surfcoat.2019.125227>
- [23] Li P, Chen K, Zhao L, Zhang H, Sun H, Yang X, Kim NH, Lee JH, Niu QJ (2019) Preparation of modified graphene oxide/polyethyleneimine film with enhanced hydrogen barrier properties by reactive layer-by-layer self-assembly. *Compos B Eng* 166:663–672. <https://doi.org/10.1016/j.compositesb.2019.02.058>
- [24] Ahmad H, Umar K, Ali SG, Singh P, Islam SS, Khan HM (2018) Preconcentration and speciation of arsenic by using a graphene oxide nanoconstruct functionalized with a hyperbranched polyethyleneimine. *Mikrochim Acta* 185:290. <https://doi.org/10.1007/s00604-018-2829-z>
- [25] Zhou X, Pan Y, Xu J, Wang A, Wu S, Shen J (2015) The carbonization of polyethyleneimine: facile fabrication of N-doped graphene oxide and graphene quantum dots. *RSC Adv* 5:105855–105861. <https://doi.org/10.1039/c5ra25173g>
- [26] Hu H, Cheng H, Zhou J, Zhu Q, Yu Y (2017) Hierarchical porous Fe₂O₃ assisted with graphene-like carbon as high-performance lithium battery anodes. *Mater Today Phys* 3:7–15. <https://doi.org/10.1016/j.mtphys.2017.10.004>
- [27] Parsamehr PS, Zahed M, Tofighy MA, Mohammadi T, Rezakazemi M (2019) Preparation of novel cross-linked graphene oxide membrane for desalination applications using (EDC and NHS)-activated graphene oxide and PEI. *Desalination* 468:114079. <https://doi.org/10.1016/j.desal.2019.114079>
- [28] Luo Q, Wirth C, Pentzer E (2020) Efficient sizing of single layer graphene oxide with optical microscopy under ambient conditions. *Carbon* 157:395–401. <https://doi.org/10.1016/j.carbon.2019.10.047>
- [29] Liu H, Zhou Y, Yang Y, Zou K, Wu R, Xia K, Xie S (2019) Synthesis of polyethyleneimine/graphene oxide for the adsorption of U(VI) from aqueous solution. *Appl Surf Sci* 471:88–95. <https://doi.org/10.1016/j.apsusc.2018.11.231>
- [30] Chen G-J, Ng KYS, Lin C-C, Selvaraj SK (2022) Effects of nitrogen-doping or alumina films on graphene as anode materials of lithium-ion batteries verified by in situ XRD. *J Nanomater* 2022:1758789. <https://doi.org/10.1155/2022/1758789>
- [31] Lim M-Y, Choi Y-S, Kim J, Kim K, Shin H, Kim J-J, Shin DM, Lee J-C (2017) Cross-linked graphene oxide membrane having high ion selectivity and antibacterial activity prepared using tannic acid-functionalized graphene oxide and polyethyleneimine. *J Membr Sci* 521:1–9. <https://doi.org/10.1016/j.memsci.2016.08.067>
- [32] Hu C, Sedghi S, Silvestre-Albero A, Andersson GG, Sharma A, Pendleton P, Rodríguez-Reinoso F, Kaneko K, Biggs MJ (2015) Raman spectroscopy study of the transformation of the carbonaceous skeleton of a polymer-based nanoporous carbon along the thermal annealing pathway. *Carbon* 85:147–158. <https://doi.org/10.1016/j.carbon.2014.12.098>
- [33] Lu H, Zhang J, Luo J, Gong W, Li C, Li Q, Zhang K, Hu M, Yao Y (2017) Enhanced thermal conductivity of free-standing 3D hierarchical carbon nanotube-graphene hybrid paper. *Compos A Appl Sci Manuf* 102:1–8. <https://doi.org/10.1016/j.compositesa.2017.07.021>
- [34] Cançado LG, Takai K, Enoki T, Endo M, Kim YA, Mizusaki H, Jorio A, Coelho LN, Magalhães-Paniago R, Pimenta MA (2006) General equation for the determination of the crystallite size L_a of nanographite by Raman spectroscopy. *Appl Phys Lett* 88. <https://doi.org/10.1063/1.2196057>
- [35] Li F, Chen Y, Li M, Liu Y, Wang B (2019) Structure evolution mechanism of polyacrylonitrile films incorporated

with graphene oxide during oxidative stabilization. 136:47701. <https://doi.org/10.1002/app.47701>

- [36] Chen X, Deng X, Kim NY, Wang Y, Huang Y, Peng L, Huang M, Zhang X, Chen X, Luo D, Wang B, Wu X, Ma Y, Lee Z, Ruoff RS (2018) Graphitization of graphene oxide films under pressure. *Carbon* 132:294–303. <https://doi.org/10.1016/j.carbon.2018.02.049>
- [37] Yang G, Yi H, Yao Y, Li C, Li Z (2020) Thermally Conductive Graphene Films for Heat Dissipation. *ACS Appl Nano Mater* 3:2149–2155. <https://doi.org/10.1021/acsanm.9b01955>

Publisher's Note Springer Nature remains neutral with regard to jurisdictional claims in published maps and institutional affiliations.

Springer Nature or its licensor (e.g. a society or other partner) holds exclusive rights to this article under a publishing agreement with the author(s) or other rightsholder(s); author self-archiving of the accepted manuscript version of this article is solely governed by the terms of such publishing agreement and applicable law.